Available online at www.sciencedirect.com
ScienceDirect
Journal of Solid State Chemistry 180 (2007) 2763–2774
JOURNAL OF SOLID STATE CHEMISTRY
www.elsevier.com/locate/jssc

Phase stabilities of monoclinic oxoborates LaB_3O_6 and GdB_3O_6 in $C121$ and $I12/a1$ phase—Energetics and chemical bonds derived from first-principles calculations

Jun Yang*, Michael Dolg

Institute of Theoretical Chemistry, University of Cologne, Greinstr. 4, 50939 Cologne, Germany

Received 9 May 2007; received in revised form 25 July 2007; accepted 30 July 2007
Available online 12 August 2007

Abstract

The computational study on the relative phase stabilities between two monoclinic polymorphs of the lanthanide-containing oxoborates LaB_3O_6 and GdB_3O_6 is presented at the first-principles density functional theory gradient-corrected B3PW level. The hypothetical monoclinic α-BiB_3O_6-like $C121$ non-centrosymmetric crystal structures were assumed for LaB_3O_6 and GdB_3O_6 and the corresponding geometries were calculated and compared with their monoclinic $I12/a1$ centrosymmetric structures. The enthalpy–pressure correlations were calculated and the first-principles chemical bonds based on the crystal orbital overlapping population were quantitatively analyzed for LaB_3O_6 and GdB_3O_6. The chemical bonds between the central cation (La (III)/Gd (III)) and coordinated oxygen atoms rather than the B–O bonds in the borate units are found to stabilize the $I12/a1$ centrosymmetric LaB_3O_6 and GdB_3O_6 structures with respect to the $C121$ non-centrosymmetric counterparts.

Keywords: BiB_3O_6; LnB_3O_6; First-principles; DFT; COOP; Chemical stability; Equation-of-states

1. Introduction

The metal-containing oxoborates have attracted wide attention and extensive investigations have been carried out to characterize the structures and properties in the past decades [1–5] mainly due to their nonlinear optical and fluorescent properties. Among the oxoborates with the chemical composition of MB_3O_6, BiB_3O_6 and the series of LnB_3O_6 (Ln = La–Lu), have been structurally resolved and found to be highly interesting. Both BiB_3O_6 and LnB_3O_6 own various polymorphs. There are four polymorphs of BiB_3O_6 identified so far, i.e., α-, β-, γ- and δ-BiB_3O_6. The α-BiB_3O_6 crystallizes under low pressure in the non-centrosymmetric monoclinic space group $C121$ and thus shows exceptional nonlinear optical properties [6–14]. High pressures have driven the formation of β- and γ-BiB_3O_6 [15] with the centrosymmetric orthorhombic space group $P2_1/n$ and δ-BiB_3O_6 [16] with again a new non-centrosymmetric modification. The ratio of $[BO_3]^{3-}$/$[BO_4]^{5-}$ units is 2:1 in α-BiB_3O_6, and changes to 1:2 in β-BiB_3O_6, while in both γ- and δ-BiB_3O_6 only $[BO_4]^{5-}$ tetrahedral units are exclusively present [16]. The binary lanthanide oxoborates LnB_3O_6 are formed in both monoclinic and orthorhombic structures. The starting of the monoclinic series of α-LnB_3O_6 with the centrosymmetric space group $I12/a1$ is marked by LaB_3O_6 ($a = 6.509$ Å, $b = 8.172$ Å, $c = 7.983$ Å, $\beta = 93.43°$) [17] and terminated at TbB_3O_6 ($a = 6.215$ Å, $b = 8.023$ Å, $c = 7.811$ Å, $\beta = 93.44°$) [18] through Ce [19], Pr [20], Nd [21], Sm [22], Eu [23] and Gd [22]. The lanthanide elements entering into the orthorhombic series of the centrosymmetric space group *Pnma* include Nd, Sm and Gd [24] as well as those smaller ones from Tb to Lu [25,26], which makes the β-LnB_3O_6 series. The second orthorhombic polymorphs with the non-centrosymmetric symmetry $Pca2_1$, called γ-LnB_3O_6, have been also grown under the high pressure for LnB_3O_6 containing the lighter lanthanide elements for La, Ce,

*Corresponding author. Fax: +49 221 4706896.
E-mail address: jyang0@uni-koeln.de (J. Yang).

0022-4596/$ - see front matter © 2007 Elsevier Inc. All rights reserved.
doi:10.1016/j.jssc.2007.07.026

Pr and Nd [27,28]. Recently the monoclinic high pressure modification of LnB_3O_6, δ-LnB_3O_6 with the centrosymmetric symmetry $P21/a$, has been found by Huppertz group for the elements La [29] and Ce [30].

In the structural series of MB_3O_6 borates, both non-centrosymmetric and centrosymmetric polymorphs have been found for BiB_3O_6 and LnB_3O_6. However, for the monoclinic series only centrosymmetric crystals of LnB_3O_6 are found and to the best of our knowledge no experiments have been successfully conducted in growing a non-centrosymmetric monoclinic phase. Therefore one question is raised for discussion that whether or not, at least theoretically, it is possible to realize non-centrosymmetric monoclinic polymorphic structure for LnB_3O_6. We note that the structures of borate units in monoclinic centrosymmetric $I12/a1$ α-LnB_3O_6 and monoclinic non-centrosymmetric $C121$ α-BiB_3O_6 indeed share several common features. First of all, both of them were crystallized under ambient pressures. Second, both α-LnB_3O_6 and α-BiB_3O_6 fall into the borate classification of $\{A/C'' = 2, BEN'' = 16, \%OH = 0, \%\Delta = 2/3P\}$ by Parthé [31] with the $[BO^3]^{3-}$/$[BO^4]^{5-}$ rations of 2:1. Each $[BO_4]^{5-}$ tetrahedron (T) is connected via two corner-sharing distorted $[BO_3]^{3-}$ triangles (Δ) on both sides, and vice versa (cf. Fig. 1). Two out of the three oxygen corners in each $[BO_3]^{3-}$ triangle are linked to $[BO_4]^{5-}$ tetrahedra and the non-bridging O atom coordinates to two cations. In addition, the resulting $[B_3O_6]^{3-}$ (i.e., $2\Delta+1T$) are the basic units in forming the infinite borate layers extending in the (100) plane for $I12/a1$ α-LnB_3O_6 and the (001) plane for $C121$ α-BiB_3O_6 (cf. Fig. 1). Consequently these borate layers of $I12/a1$ α-LnB_3O_6 and $C121$ α-BiB_3O_6 are alternating along the a and c direction, respectively. However, the coordination polyhedra around central cations are substantially different for α-LnB_3O_6 and α-BiB_3O_6. The central Ln is irregularly coordinated by 10 O atoms and the resultant $[LnO_{10}]^{17-}$ infinite chains run along the c-axis. The Bi (III) is six-fold-coordinated in α-BiB_3O_6 forming $[BiO_6]^{9-}$ units in which four shortest Bi–O bonds stay at the same side of Bi (III) (2.086 and 2.390 Å) and other two bonds remain relatively far away at the other side of Bi (III) (2.632 Å). Therefore one can expect that the structural deviation of α-LnB_3O_6 from the non-centrosymmetric α-BiB_3O_6-like structure would possibly stem from the coordination polyhedra of the central cations since their borate units are spatially arranged in a similar way to a great extent.

In view of the non-centrosymmetric structure of α-BiB_3O_6 and the similar ionic radii and electronegativities between Ln (III) and Bi (III), one simple way is to substitute Ln (III) for Bi (III) in the original $C121$ α-BiB_3O_6 and study at the first-principles level the relative phase stability along with related mechanism between the assumed α-BiB_3O_6-like LnB_3O_6 structure, i.e., the $C121$ space group, and the α-LnB_3O_6 structure, i.e., the $I12/a1$ space group. To this end, we rather take LaB_3O_6 and GdB_3O_6 as two examples which contain lanthanide elements with similar ground state valence electronic configurations $5s^25p^65d^16s^2$ and $4f^75s^25p^65d^16s^2$, respectively, to seek the possible answer without losing general features, than go through the entire series in order to avoid the unattainable computational time.

2. Theoretical methods

The hypothetical monoclinic $C121$ structures of LaB_3O_6 and GdB_3O_6 were generated in the manner that the Bi cation in BiB_3O_6 was replaced by La and Gd for LaB_3O_6 and GdB_3O_6, respectively, while the original lattice parameters and atomic coordinates of BiB_3O_6 were retained for LaB_3O_6 and GdB_3O_6. Optimizations of all

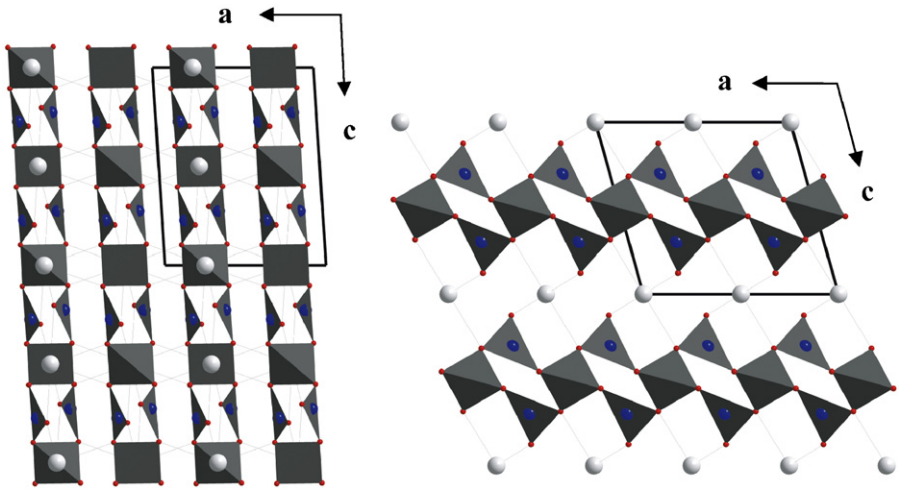

Fig. 1. The (010) plane views for two monoclinic crystallographic structures of α-MB_3O_6 (M = Ln, Bi). The α-LnB_3O_6 presents the centrosymmetric $I12/a1$ space group (left) and the α-BiB_3O_6 the non-centrosymmetric $C121$ space group (right). The metal, boron and oxygen atoms are indicated by the large sphere, the medium sphere and the small sphere, respectively. The polyhedral $[B_3O_6]^{3-}$ sheet (dark gray areas) contains triangular $[BO_3]^{3-}$ (Δ) and tetrahedral $[BO_4]^{5-}$ (T) units with a ratio 2Δ:1T.

geometric parameters for LaB_3O_6 and GdB_3O_6 were subsequently carried out under the $C121$ symmetry constraint in the density functional theory (DFT) approach for the B3PW hybrid functional [32–35]. The monoclinic $I12/a1$ structures of LaB_3O_6 and GdB_3O_6 were taken from the experimental data and fully optimized. The geometry optimizations were performed by using the conjugate gradient code LoptCG [36] modified by us for full optimizations of both lattice parameters and atomic coordinates in connection with the package CRYSTAL03 [37]. For each displaced lattice parameter, the atomic coordinates were relaxed analytically by fulfilling three criteria, i.e., between optimization steps the root mean square (RMS) of energy change, gradient change and displacement change should stay less than 10^{-7}, 0.0003 and 0.0012 a.u., respectively. The numerical gradients were obtained for lattice parameters and the optimization convergence was achieved by meeting the thresholds for the RMS-weighted-norm of 0.001 and maximum-weighted-derivatives of 0.003.

The following tolerances were employed in the evaluation of the infinite Coulomb and HF exchange series: 10^{-7} for the Coulomb overlap, HF exchange overlap, Coulomb penetration and the first exchange pseudo-overlap; 10^{-14} for the second exchange pseudo-overlap. The Fock matrix has been diagonalized at 24 **k**-points within the irreducible Brillouin zone corresponding to a shrinking factor of 4 in the Monkhorst net [38]. In order to improve the convergence, a negative energy shift of 1.0 a.u. to the diagonal Fock/KS matrix elements of the occupied orbitals was added to reduce their coupling to the unoccupied set and maintained after the diagonalization. A very accurate extra-large grid consisting of 75 radial points and 974 angular points was employed in the DFT calculations, where Becke grid point weights [39] were chosen.

The crystal-orbital-adapted valence basis sets previously derived by us [40] were applied to La and Gd cations in association with the energy-consistent scalar-relativistic 4*f*-in-core ECPs [41–43] of the Stuttgart-Cologne variety which provide 11 electrons in the valence configuration of $5s^25p^65d^16s^2$. The Dunning contraction (11*s*, 6*p*)/[5*s*, 3*p*] [44] and 6-311**G*** basis sets [45] were employed for oxygens and borons, respectively. One additional *d* polarization function with the energetically optimized exponent of 0.87 was added to the (11*s*, 6*p*)/[5*s*, 3*p*] contractions of the oxygens in all calculations.

We have gauged the relative phase stabilities for the $C121$ and $I12/a1$ monoclinic phases corresponding to 0 K by the following two means. The first straightforward way is to calculate and compare the enthalpies of $C121$ and $I12/a1$ phases, following the thermodynamics principle, i.e., the lower enthalpy favors the stable structure. To this end, the electronic energies for crystals with fully relaxed atomic positions in isotropically expanded and compressed unit cells along the directions of three fixed lattice constants were calculated and fitted by the Birch–Murnaghan equation [46,47] (cf. Eq. (1)) with respect to the cell volumes V:

$$E(V) = E_0 + \frac{9}{16} V_0 B_0 \left\{ \left[\left(\frac{V_0}{V} \right)^{2/3} - 1 \right]^3 B_0' + \left[\left(\frac{V_0}{V} \right)^{2/3} - 1 \right]^2 \left[6 - 4 \left(\frac{V_0}{V} \right)^{2/3} \right] \right\}, \quad (1)$$

where E_0, V_0 and B_0 refer to the total electronic energy, volume and the bulk modulus at the equilibrium structure, respectively. The external pressure was calculated according to Eq. (1):

$$P(V) = -\left[\frac{\partial E(V)}{\partial V} \right]_{T=0\,\mathrm{K}} = \frac{3}{2} B_0 \left[\left(\frac{V_0}{V} \right)^{7/3} - \left(\frac{V_0}{V} \right)^{5/3} \right] \times \left\{ 1 + \frac{3}{4} (B_0' - 4) \left[\left(\frac{V_0}{V} \right)^{2/3} - 1 \right] \right\}. \quad (2)$$

In our case, the zero-point vibrational energy correction was excluded to keep the calculation at an acceptable computational expense. The enthalpy is thereby obtained as

$$H(V) = E(V) + VP(V). \quad (3)$$

The second approach relates the relative structural stability to the chemical bonds. In view of the classic picture of chemistry, a chemically stable compound needs to contain overall more intensive bonding along with overall less antibonding at the equilibrium structure than a chemically less stable compound if no external pressure is applied. The strength of chemical bonds can be measured by the crystal orbital overlap population (COOP) $O^{\mathbf{G}}_{\alpha\beta}(\varepsilon)$ in Eq. (4) between two atom-centered orbital sets α in the reference cell (0, 0, 0) and β in the unit cell **G**:

$$O^{\mathbf{G}}_{\alpha\beta}(\varepsilon) = \sum_{u\in\alpha} \sum_{v\in\beta} S^{\mathbf{G}}_{uv} \frac{\mathrm{d}P^{\mathbf{G}}_{uv}(\varepsilon)}{\mathrm{d}\varepsilon}, \quad (4)$$

where $S^{\mathbf{G}}_{uv}$ is the element of the overlap matrix for the atomic orbital u in the reference cell (0, 0, 0) and v in the cell g, and $P^{\mathbf{G}}_{uv}(\varepsilon)$ is the element of the density matrix projected out up to the energy level ε. COOP describes the density of bonding and antibonding interactions between specific orbitals at a given energy in solids, while its integral intensity for a certain energy interval denotes the relative bond strength within this energy interval. Regions with positive COOP contributions are bonding, regions with negative COOP contributions are antibonding, and zero COOP contributions are nonbonding. We note that in addition to COOP originally introduced by Hughbanks and Hoffmann [48] several other methods such as crystal orbital Hamilton population (COHP) [49] and balanced crystal orbital overlap population (BCOOP) [50] are alternative options.

3. Results and discussions

3.1. Optimized geometry structures

The calculated structural parameters for both $C121$ and $I12/a1$ phases of LaB_3O_6 and GdB_3O_6 are given in Table 1. For the $C121$ structures, the shrunk lattice constant a as well as expanded lattice constants b and c are observed for assumed LaB_3O_6 and GdB_3O_6 compared to those of α-BiB_3O_6. The Ln–O bond lengths stay closer to each other than those of BiB_3O_6.

3.2. Electronic structures

The electronic structures are examined by discussing the DOS for the $C121$ and $I12/a1$ phases of LaB_3O_6 and GdB_3O_6 (cf. Figs. 2(a), 2(b), 3(a) and 3(b)). First of all, both the $C121$ and $I12/a1$ phases suggest similar occupied state distributions with respect to the energy level. Sharp and strong La s states dominate the energy level at about -39 eV, and Gd s states at about -48 eV. The top of the valence states is contributed by strong O $2p$ states, weak but broad Ln d states as well as minor O $2s$ and Ln sp states. The state penetration is found between O $2s$ and $2p$ orbitals, which implies that both O $2s$ and $2p$ states participate into the orbital interactions with the cations. Second, the split Ln p states shift down the energy level from La to Gd. Consequently the Gd p states turn to have the almost complete overlapping with the O $2s$ states, which is much more pronounced than La p states. The separations within occupied La p states in the $C121$ and $I12/a1$ phases are 2.7 and 3.1 eV, which are considerably decreased to 0.3 and 0.06 eV for Gd p states, respectively. One can imagine that for the heavier lanthanide elements than Gd, their p states would energetically stay no higher than the O $2s$ energy levels if they are condensed into LnB_3O_6 crystals. We note that the experimental $I12/a1$ structures for Ln = Dy–Lu are still missing, which may be supported by the distinct electronic structures of the monoclinic $I12/a1$ α-LnB_3O_6 between Ln = La–Tb and Ln = Dy–Lu as the consequence of the down-shifting energetic levels of Ln p states relative to O $2p$ states. However, the experience based on the calculated electronic structures of $I12/a1$ α-LnB_3O_6 needs to be reconsidered with great care in cases of other polymorphs of LnB_3O_6, for example, the orthorhombic $Pnma$ β-LnB_3O_6 with both Ln = Nd, Sm and Gd [24] and Ln = Tb–Lu [25,26].

3.3. Energetics and stabilities

The Birch–Murnaghan fittings of the energy points against various ratios of the equilibrium volume to deformed volumes are provided in Figs. 4 and 5. It is clear that at the equilibrium structures with $V_0/V = 1.0$, the $I12/a1$ phase stands energetically lower than the $C121$ phase by 0.0198 a.u. (i.e., 12.4 kcal/mol) for LaB_3O_6 and 0.0099 a.u. (i.e., 6.2 kcal/mol) for GdB_3O_6. Therefore, from the energy point of view, LaB_3O_6 and GdB_3O_6 seem to preferably crystallize into the $I12/a1$ phase rather than the $C121$ one, which agrees well with the experimental observation that no $C121$ LnB_3O_6 phase has yet been confirmed. In the next section, we try to explain the reason responsible for such occurrences by manifesting their chemical bonds. The fitted parameters of the Birch–Murnaghan Eq. (1) are given in Table 2. The fitted equilibrium volumes and energies differ from the values derived from the direct DFT full geometry optimization by only ~0.5, ~0.1, ~0.2 and ~0.1 Å^3 as well as 6×10^{-5}, 1×10^{-5}, 6×10^{-5} and 5×10^{-5} a.u. for the LaB_3O_6 ($C121$, $I12/a1$) and GdB_3O_6 ($C121$, $I12/a1$) phases, respectively. These minor deviations indicate the sufficient accuracies obtained by optimizing only the atomic coordinates but fixing lattice parameters for Birch–Murnaghan fittings. The

Table 1
The comparisons between the experimental and calculated lattice parameters and bond distances (Å) for both the $C121$ and $I12/a1$ phases of LaB_3O_6 and GdB_3O_6

$C121$ phase	Lattice parameters				M–O					B–O in $[BO_3]^{3-}$			B–O in $[BO_4]^{5-}$	
	a	b	c	β	d_1	d_2	d_3			d_4	d_5	d_6	d_7	d_8
LaB_3O_6 Cal.	6.530	5.980	6.941	102.8	2.375	2.502	2.483			1.339	1.385	1.409	1.457	1.490
GdB_3O_6 Cal.	6.324	6.027	6.803	100.4	2.285	2.350	2.406			1.336	1.386	1.405	1.448	1.487
α-BiB_3O_6 Exp. [9]	7.116	4.993	6.508	105.6	2.086	2.390	2.632			1.339	1.365	1.411	1.436	1.487
$I12/a1$ phase	Lattice parameters				M–O					B–O in $[BO_3]^{3-}$			B–O in $[BO_4]^{5-}$	
	a	b	c	β	d_1	d_2	d_3	d_4	d_5	d_6	d_7	d_8	d_9	d_{10}
α-LaB_3O_6 Exp. [17]	7.983	8.172	6.509	93.4	2.428	2.565	2.601	2.618	2.848	1.336	1.368	1.396	1.501	1.503
α-LaB_3O_6 Cal.	7.999	8.240	6.607	93.2	2.459	2.560	2.663	2.664	2.874	1.332	1.390	1.423	1.457	1.496
α-GdB_3O_6 Exp. [22]	7.80	8.02	6.28	93.0	2.282	2.471	2.537	2.638	2.693	1.367	1.369	1.373	1.474	1.498
α-GdB_3O_6 Cal.	7.867	8.106	6.362	93.3	2.358	2.498	2.529	2.549	2.851	1.331	1.388	1.414	1.453	1.488

All the calculated values were derived based on the DFT B3PW results.

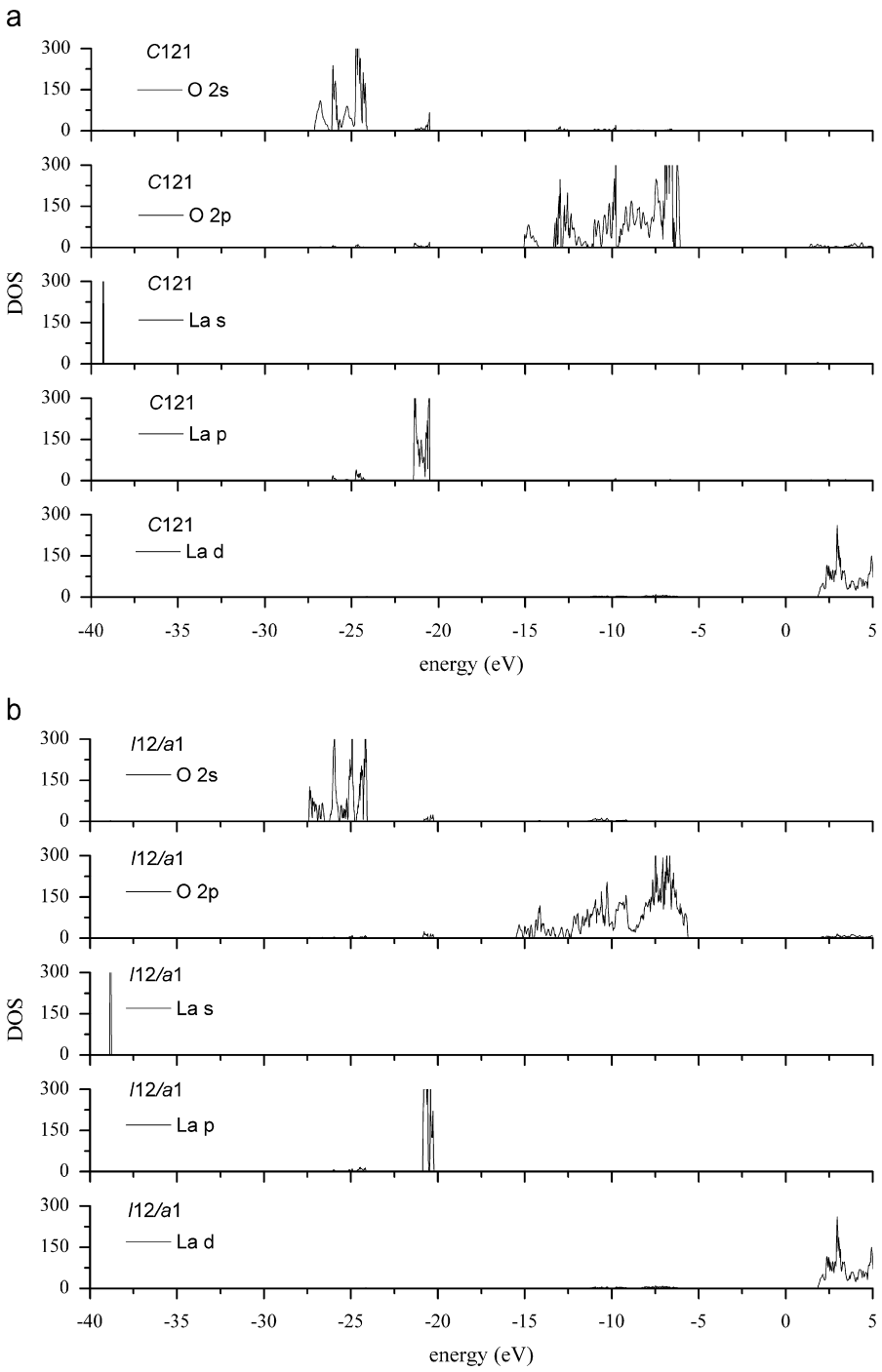

Fig. 2. The l-momentum projected densities of states (DOS) for LaB_3O_6 in $C121$ (a) and $I12/a1$ phases (b).

bulk moduli of the realized $I12/a1$ phases are over 50% larger than those of the hypothetical $C121$ phases.

Apart from the equilibrium structures, it is interesting to learn that whether the application of external pressure favors the stability of the $C121$ phase, or not. The calculated enthalpies corresponding to 0 K are plotted in Figs. 6 and 7 for various pressures. It is found that the most stable structure in either the $C121$ or the $I12/a1$ phase takes place at the ambient pressure. The higher pressure would actually further cause a higher instability of the individual structure since the corresponding enthalpy is increased. It appears in Figs. 6 and 7 that the $C121$ phases of both LaB_3O_6 and GdB_3O_6 are even more instable than the $I12/a1$ ones at higher pressures. It is highly unlikely to find a converging point at a certain pressure in the enthalpy–pressure curves for the $C121$ and $I12/a1$ phases where the former could be viewed to start the transition to the latter phase.

We expect that, due to the similarities of the lanthanide elements, the other monoclinic lanthanide borates LnB_3O_6

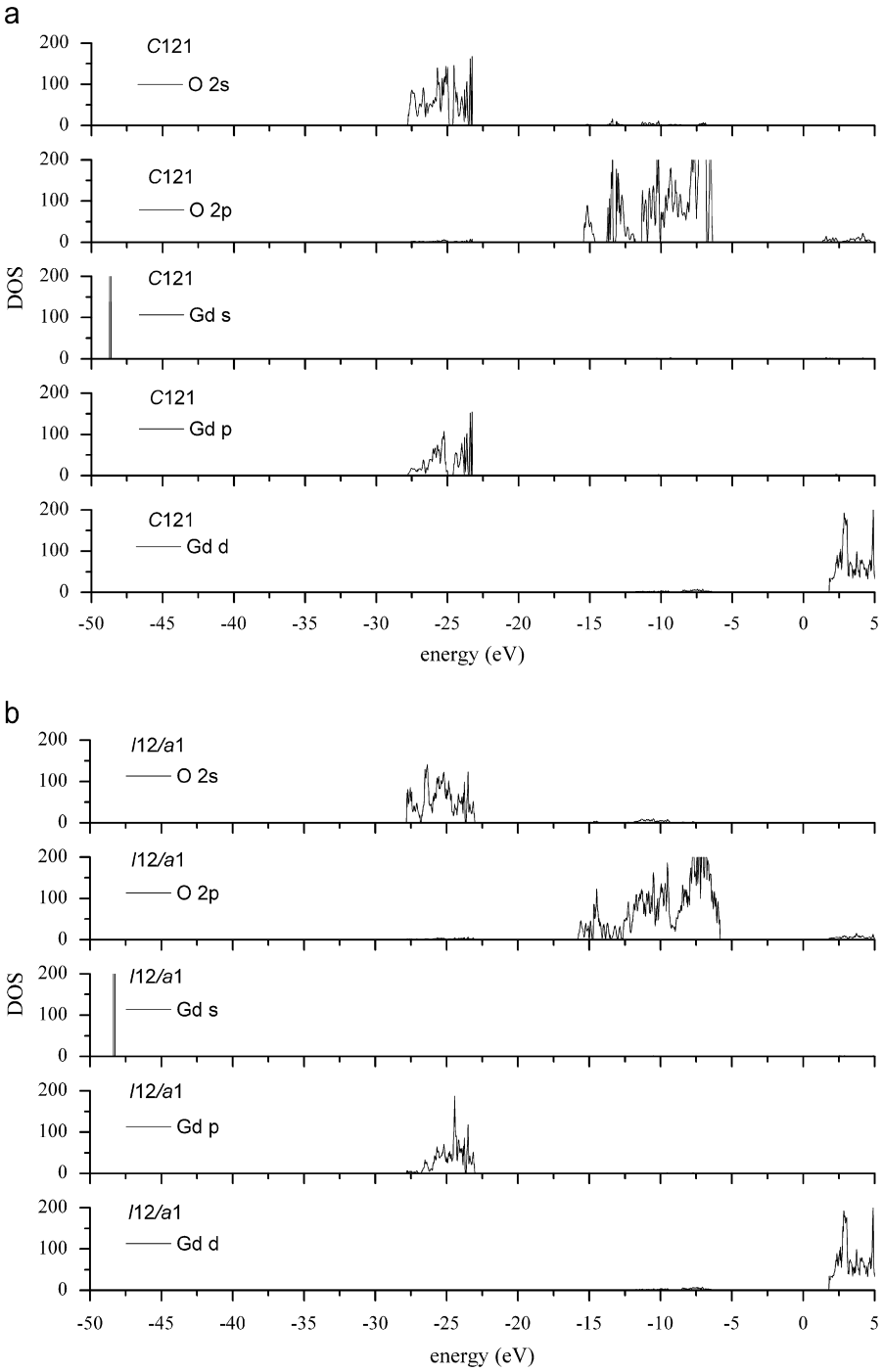

Fig. 3. The l-momentum projected densities of states (DOS) for GdB_3O_6 in $C121$ (a) and $I12/a1$ (b) phases.

(Ln = Ce, Pr, Nd, Sm and Eu) would present the same trend of relative stabilities between the $C121$ and $I12/a1$ phases as the cases of LaB_3O_6 and GdB_3O_6, i.e., the monoclinic LnB_3O_6 would occur with the centrosymmetric $I12/a1$ structures rather than the non-centrosymmetric $C121$ ones. However, this does not necessarily exclude the case where a non-centrosymmetric structure is also possible to LnB_3O_6. As a matter of fact, the orthorhombic series of γ-LnB_3O_6 [27,28] has been grown to be non-centrosymmetric, which holds the same structure as δ-BiB_3O_6 [16]. In addition, we have to point out that the current computational investigation on the relative stabilities has not considered any temperature effects, e.g., the thermal vibrations of nuclei may also have notable contributions to the crystal stabilities.

3.4. Chemical bonds and stabilities

The integral COOP intensities for the B–O bonds in $[BO_3]^{3-}$ and $[BO_4]^{5-}$ borate units are given in Table 4. The

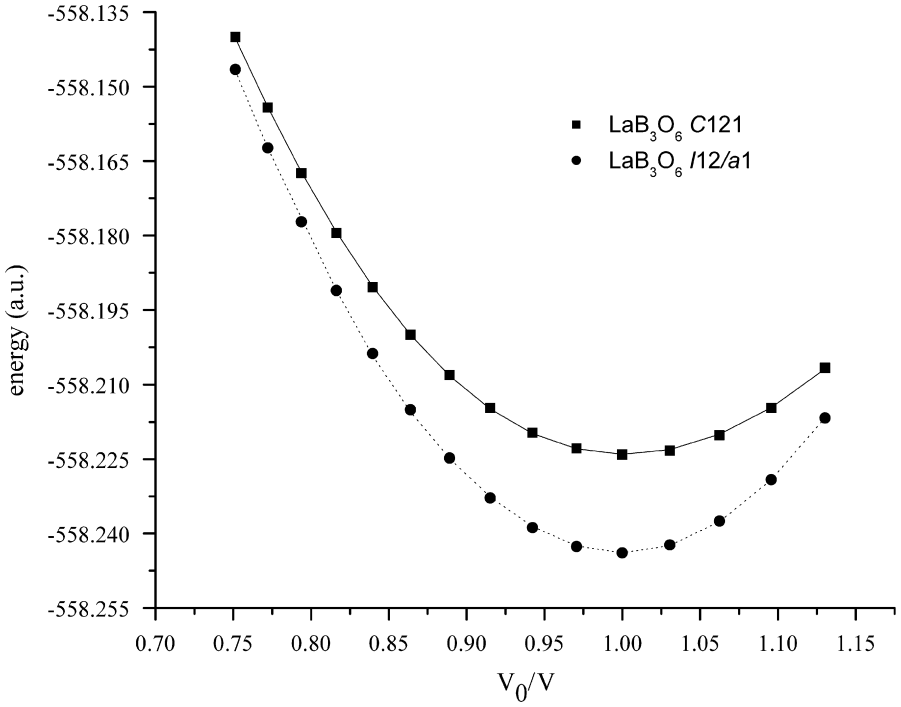

Fig. 4. The Birch–Murnaghan fittings for the total electronic energies of LaB_3O_6 with respect to the volume ratios. V_0 is the volume of a primitive cell at the equilibrium structure (1 a.u. = 627.510 kcal/mol).

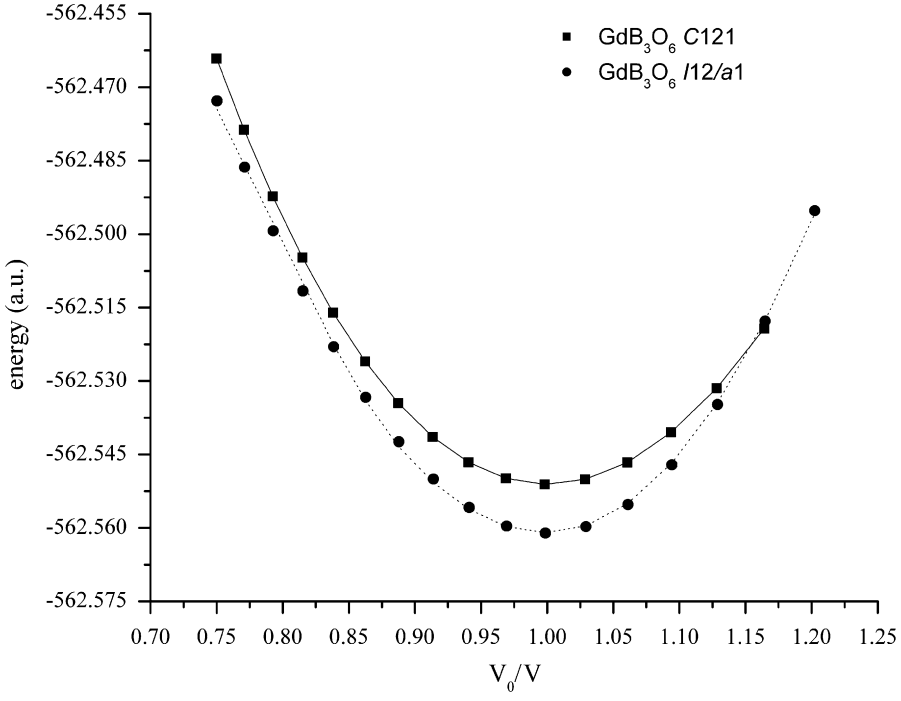

Fig. 5. The Birch–Murnaghan fittings for the total electronic energies of GdB_3O_6 with respect to the volume ratios. V_0 is the volume of a primitive cell at the equilibrium structure (1 a.u. = 627.510 kcal/mol).

B–O bonds in triangular $[BO_3]^{3-}$ units appear to be the occupied bonding orbitals and those in tetrahedral $[BO_4]^{5-}$ units are contributed by both relatively strong occupied bonding and weak occupied antibonding interactions. It looks that these borate units are comparably stable in both the $C121$ and $I12/a1$ LnB_3O_6 borates regardless of the central cations. Therefore the B–O bonds in borate units are not mainly responsible for the instability of $C121$ LnB_3O_6.

The Mulliken populations on Ln are shown in Table 3. Since the shells with a main quantum number smaller than

5 are taken as effective core potential of Ln, the valence shell electron population has a $5s^25p^65d^16s^2$ configuration as reference (11 electrons). It is well-known that the compact 4*f*-shell shields the nuclear-charge quite efficiently and only small differences are observed in the populations of the outer valence orbitals when comparing La and Gd. In all cases, the *s*-population is about 2.0, which suggests that the 6*s* orbital is ionic and the main electron donor in these crystalline compounds while the 5*s* orbital remains the double electron occupancy. The *p*-population is about 6.0 and fully occupied. The *d*-population is about 0.7 and suggests that a significant amount of *d* orbitals is left unoccupied. Therefore the 6*d* orbital is less ionic than 6*s* and 6*p* orbitals. This is in line with the state distributions of La and Gd in Figs. 2 and 3. The total atomic charge on Ln is about 2.2, which implies the substantial covalent characteristics of central Ln metals.

Table 2
The calculated bulk modulus (B_0), its first derivative (B_0'), the equilibrium volume (V_0) and the lowest energy (E_0) in both the *C*121 and *I*12/*a*1 phases for LaB_3O_6 and GdB_3O_6

Crystals	Parameters	*C*121	*I*12/*a*1
LaB_3O_6	B_0 (GPa)	76.78	125.95
	B_0'	3.45	4.92
	V_0 (Å^3)	131.696 (132.133)	108.828 (108.700)
	E_0 (a.u.)	−558.22411 (−558.22405)	−558.24388 (−558.24387)
GdB_3O_6	B_0 (GPa)	85.80	130.82
	B_0'	3.85	5.79
	V_0 (Å^3)	127.262 (127.492)	101.128 (101.257)
	E_0 (a.u.)	−562.55111 (−562.55117)	−562.56105 (−562.56100)

The numbers in the brackets denote the values of equilibrium volumes and energies derived from the DFT calculations.

The COOP plots for the Ln–O bonds including the Ln *s*, *p* and *d* orbital contributions in LnB_3O_6 of the *C*121 and *I*12/*a*1 phases are presented in Figs. 8(a), 8(b), 9(a) and 9(b), respectively. In the *C*121 phase, the Ln *s*–O and Ln *p*–O bonds form both occupied bonding and occupied antibonding orbitals below the Fermi level. The *C*121 Ln *s*–O antibonding peaks are significant at the top of the valence states (top figures in Figs. 8(a) and 9(a)), while the Ln *s*–O bonding peaks are sharp and weak at the deepest energy level. Both Ln *p*–O bonding and antibonding peaks are much stronger than the Ln *s*–O counterparts. This can be understood as a consequence that, on one hand, Ln 5*p* orbitals are more spatially extensive than Ln 5*s* orbitals, and on the other hand, Ln 6*s* orbitals are left unoccupied in LnB_3O_6 crystals due to the null Mulliken population at Ln 6*s* orbitals. The Ln *d*–O orbital couplings directly result in the occupied Ln *d*–O bonding orbitals and the corresponding antibonding orbitals are unoccupied. One can further see in Table 5 that the Ln *d*–O bonds are evidently stronger than Ln *p*–O and Ln *s*–O bonds, which is in accordance with the fact that the Ln 5*d* orbitals are more spatially diffuse and thus intend to have more pronounced interactions with the orbitals of oxygen ligands than Ln 5*p* and Ln 5*s* orbitals.

The COOP plots for the *I*12/*a*1 phases present the tremendously different features from those for the *C*121 phases. First of all, in *I*12/*a*1 phases the Ln *s* states can be viewed as almost purely ionic states since the *I*12/*a*1 Ln *s*

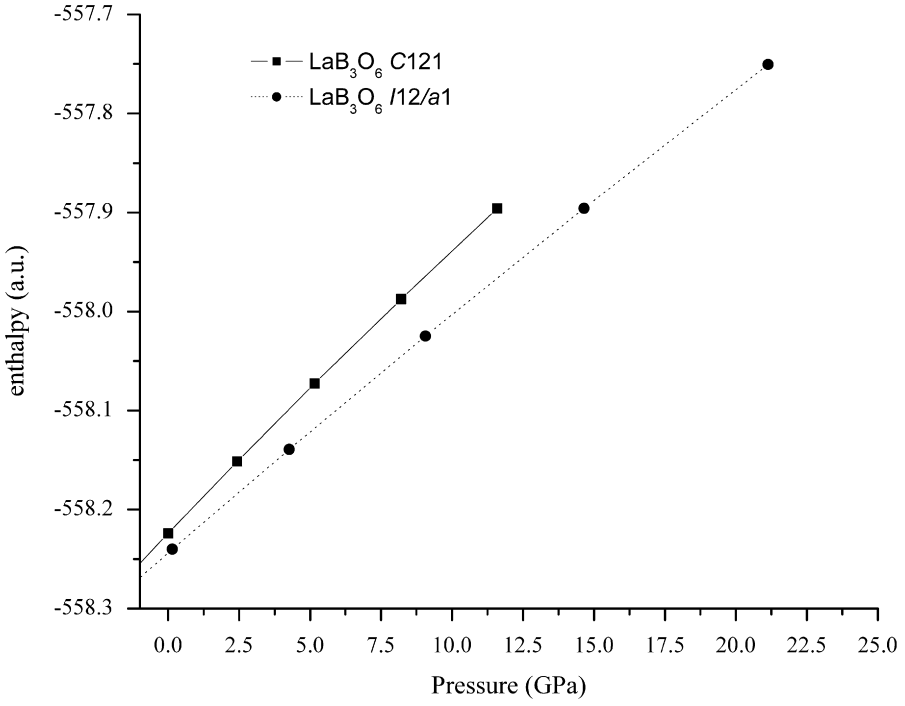

Fig. 6. The calculated enthalpies against the external pressures derived by the third-order Birch–Murnaghan equation of state for LaB_3O_6 (1 a.u. = 627.510 kcal/mol).

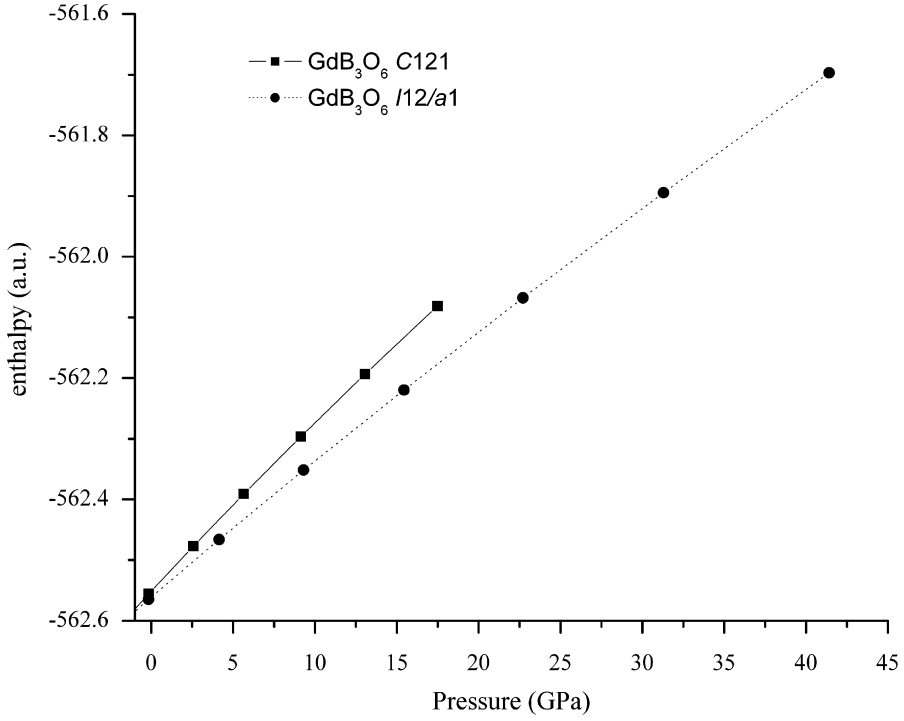

Fig. 7. The calculated enthalpies against the external pressures derived by the third-order Birch–Murnaghan equation of state for GdB_3O_6 (1 a.u. = 627.510 kcal/mol).

Table 3
Mulliken shell populations and atomic charges (Q) on Ln in LnB_3O_6 (Ln = La, Gd)

	s		*p*		*d*		*Q*	
	*C*121	*I*12/*a*1	*C*121	*I*12/*a*1	*C*121	*I*12/*a*1	*C*121	*I*12/*a*1
La	2.0	2.1	6.0	6.0	0.7	0.7	2.3	2.2
Gd	2.1	2.1	6.0	6.1	0.7	0.7	2.2	2.1

Table 4
The integral COOP intensities for the strength of B–O bonds for one Ln-coordination polyhedron

Compounds	Space group	B–O bonds	Bonding	Antibonding	Net
LaB_3O_6	*C*121	In $[BO_3]^{3-}$ triangles	+2.30	0.00	+2.30
		In $[BO_4]^{5-}$ tetrahedral	+1.08	−0.06	+1.02
		Overall	+3.38	−0.06	+3.32
	*I*12/*a*1	In $[BO_3]^{3-}$ triangles	+2.09	0.00	+2.09
		In $[BO_4]^{5-}$ tetrahedral	+0.89	−0.11	+0.78
		Overall	+2.98	−0.11	+2.87
GdB_3O_6	*C*121	In $[BO_3]^{3-}$ triangles	+2.34	0.00	+2.34
		In $[BO_4]^{5-}$ tetrahedral	+1.04	−0.05	+0.99
		Overall	+3.38	−0.05	+3.33
	*I*12/*a*1	In $[BO_3]^{3-}$ triangles	+2.00	0.00	+2.00
		In $[BO_4]^{5-}$ tetrahedral	+0.89	−0.12	+0.77
		Overall	+2.89	−0.12	+2.77

orbitals avoid bonding to O atoms (cf. Table 5). This is further supported by the Mulliken populations that the *I*12/*a*1 Ln 6*s* states are unoccupied and the occupancy at the *I*12/*a*1 Ln 5*s* states is 2.0. Second, a delicate structural variation of Ln *p*–O antibonding peaks is found at −12 eV to −15 eV for both LaB_3O_6 and GdB_3O_6. This Ln *p*–O antibonding COOP within this energy interval becomes almost zero in the *I*12/*a*1 phase, while a negative peak

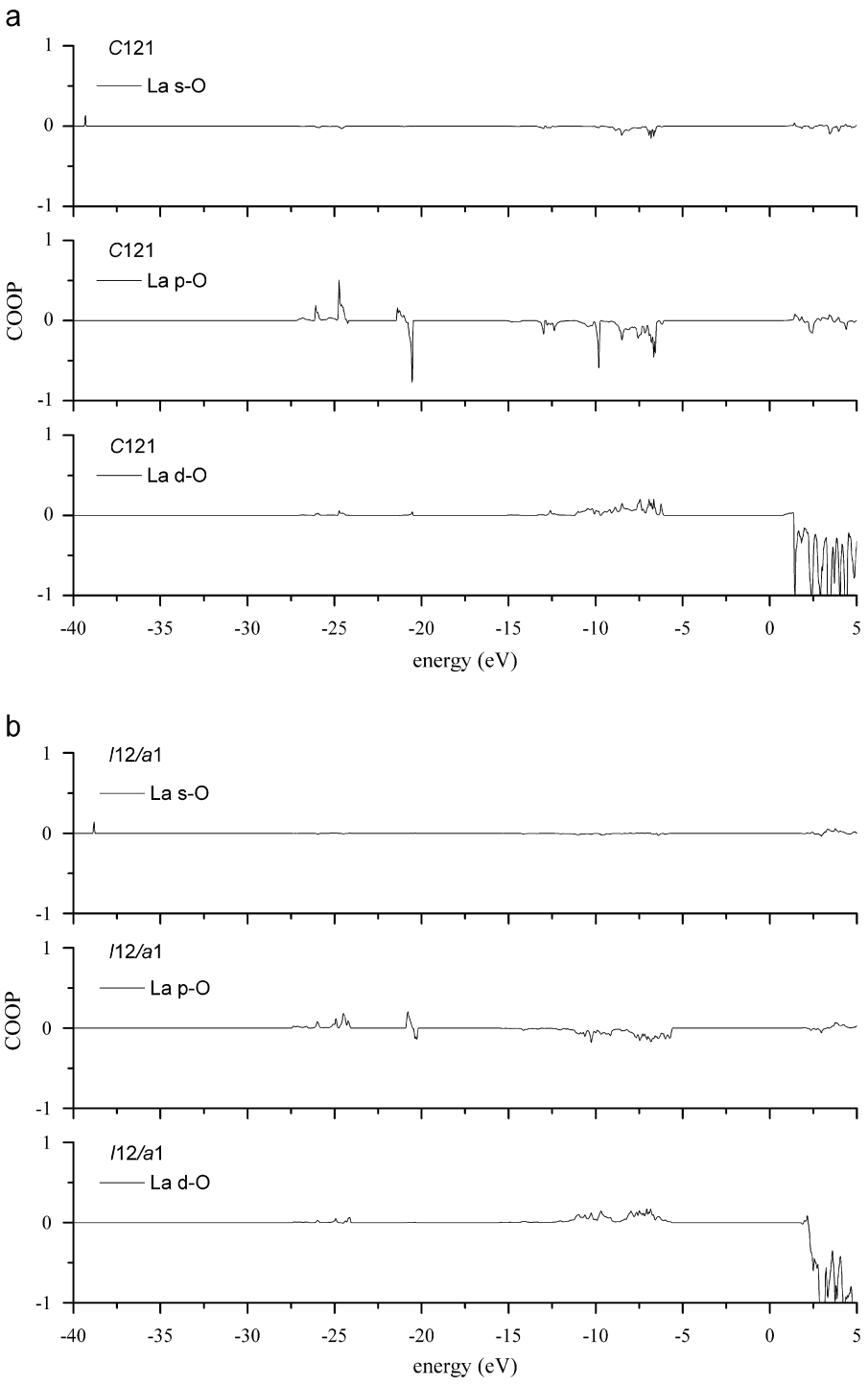

Fig. 8. The COOP plots of the La–O bonds for LaB_3O_6 in the $C121$ (a) and $I12/a1$ (b) phases for one La-coordination polyhedron.

exists in the hypothetical $C121$ phase. The above two contrasts between the $C121$ and $I12/a1$ LnB_3O_6 essentially indicate the origin of the instabilities of the $C121$ LnB_3O_6 structures compared to $I12/a1$ ones in terms of chemical bonds. The overall La–O and Gd–O bonding strengths seem to remain almost unchanged around $+0.61$ and $+0.70$ between their $C121$ and $I12/a1$ polymorphs. However, the net $I12/a1$ La–O and Gd–O bonds are significantly intensified compared to the net $C121$ La–O and Gd–O bonds due to the greatly reduced overall La–O and Gd–O antibonding strengths from -0.81 and -0.65 in $C121$ to -0.52 and -0.39 in $I12/a1$, respectively. The Mulliken population shows that there are 0.7 electrons in the La $5d$ orbitals. This occupied Ln d–O bonding interactions remain the almost invariant strength in both the $C121$ and $I12/a1$ structures and are particularly

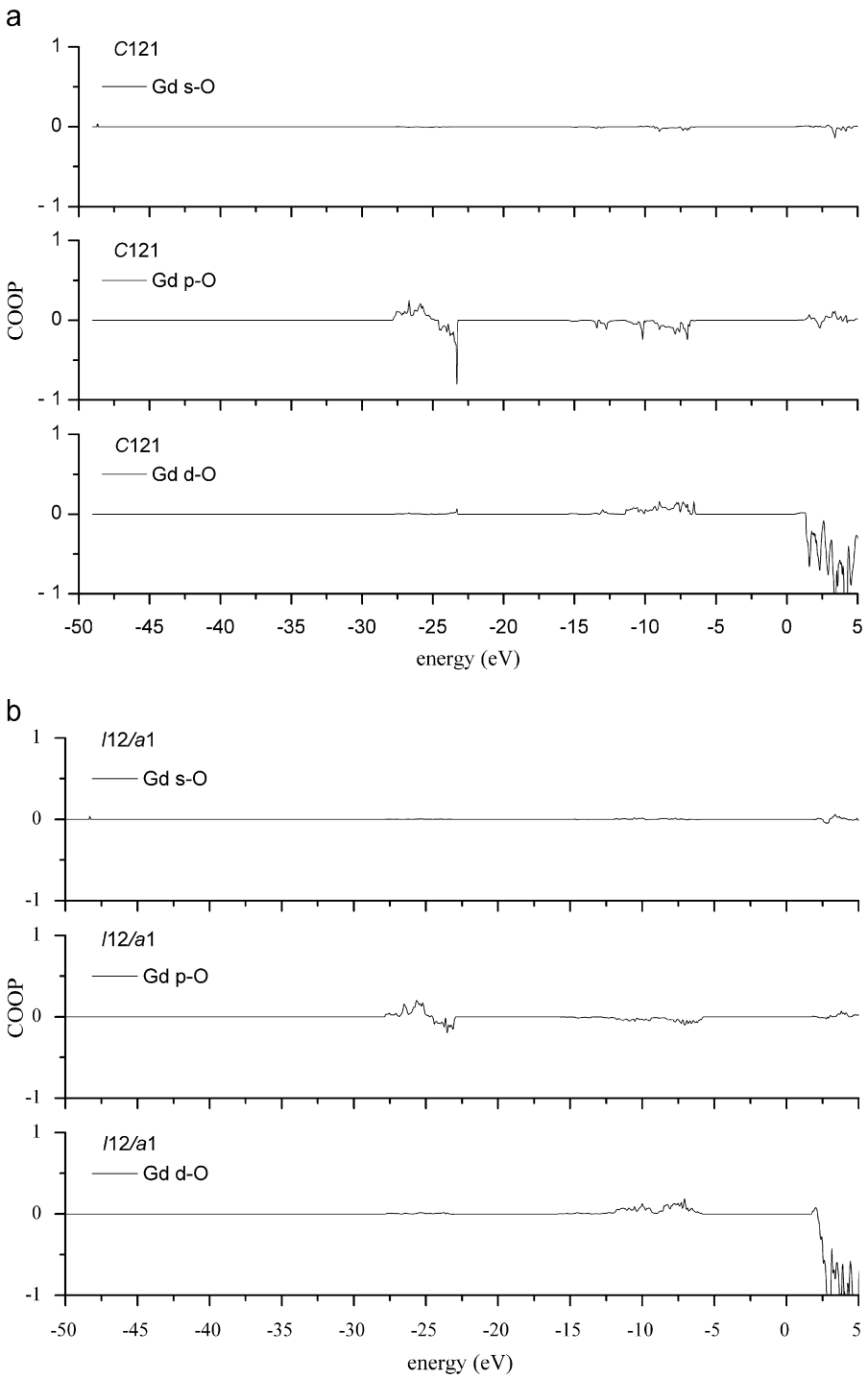

Fig. 9. The COOP plots of the Gd–O bonds for GdB_3O_6 in the $C121$ (a) and $I12/a1$ (b) for one Gd-coordination polyhedron.

important to further compensate the Ln p–O antibonding effects, which in turn stabilizes the $I12/a1$ LnB_3O_6 structure.

4. Conclusions

The LnB_3O_6 borates cannot be only viewed as the purely ionic solids, which otherwise cannot explain the relative stabilities of LnB_3O_6 between the $C121$ and $I12/a1$ phases by merely Ln^{3+}–O^{2-} electrostatic interactions. The Ln–O covalent bonds are so dominant for LnB_3O_6 that they determine the structural stability even more remarkable than the Ln^{3+}–O^{2-} electrostatic interactions. Nevertheless, the ionicity of the $I12/a1$ LaB_3O_6 is much stronger than of $I12/a1$ GdB_3O_6, since the net La–O covalent bond strength is only $+0.09$ while that of Gd–O is $+0.32$. This is interpreted as the consequence of the lanthanide contraction which leads to the substantially shorter Gd–O

Table 5
The integral COOP intensities for the strength of Ln–O bonds for one Ln-coordination polyhedron

Compounds	Space groups	Ln–O bonds	Bonding	Antibonding	Net
LaB_3O_6	*C*121	*s*–O	+0.01	−0.16	−0.15
		p–O	+0.18	−0.65	−0.47
		d–O	+0.41	0.00	+0.41
		Overall	+0.60	−0.81	−0.21
	*I*12/*a*1	*s*–O	+0.01	−0.04	−0.03
		p–O	+0.14	−0.48	−0.34
		d–O	+0.46	0.00	+0.46
		Overall	+0.61	−0.52	+0.09
GdB_3O_6	*C*121	*s*–O	+0.01	−0.06	−0.05
		p–O	+0.28	−0.59	−0.31
		d–O	+0.40	0.00	+0.40
		Overall	+0.69	−0.65	+0.04
	*I*12/*a*1	*s*–O	+0.04	0.00	+0.04
		p–O	+0.22	−0.39	−0.17
		d–O	+0.45	0.00	+0.45
		Overall	+0.71	−0.39	+0.32

distances and more crystal orbital overlapping in *I*12/*a*1 GdB_3O_6 than in *I*12/*a*1 LaB_3O_6. The stabilities of *I*12/*a*1 α-LaB_3O_6 and α-GdB_3O_6 originate from the occupied bonding Ln *d*–O orbitals as well as the reduced occupied Ln *sp*–O antibonding orbitals compared to the hypothetical *C*121 structures of LaB_3O_6 and GdB_3O_6.

References

[1] P. Becker, Adv. Mater. 10 (1998) 979.
[2] J. Weidelt, Z. Anorg. Allg. Chem. 26 (1970) 374.
[3] H.U. Bambauer, J. Weidelt, J.-St. Ysker, Z. Kristallogr. 130 (1969) 207.
[4] D.A. Keszler, Curr. Opin. Solid State Mater. Sci. 1 (1996) 204.
[5] T. Sasaki, Y. Mori, M. Yoshinura, Y.K. Yap, T. Kamimura, Mater. Sci. Eng. 1 (2000) 30.
[6] P. Becker, C. Wickleder, Cryst. Res. Technol. 36 (2001) 2737.
[7] B. Teng, Z.P. Wang, H.D. Jiang, X.F. Cheng, H. Liu, X.B. Hu, S.M. Dong, J.Y. Wang, Z.S. Shao, J. Appl. Phys. 91 (2001) 3618.
[8] S. Haussühl, L. Bohatý, P. Becker, Appl. Phys. A 82 (2006) 495.
[9] R. Fröhlich, L. Bohatý, J. Liebertz, Acta Crystallogr. C 40 (1984) 343.
[10] L. Bohatý, J. Liebertz, Z. Kristallogr. 170 (1985) 18.
[11] P. Becker, J. Liebertz, L. Bohatý, J. Cryst. Growth 203 (1999) 149.
[12] H. Hellwig, J. Liebertz, L. Bohatý, Solid State Commun. 109 (1998) 249.
[13] H. Hellwig, J. Liebertz, L. Bohatý, J. Appl. Phys. 88 (2000) 240.
[14] I.V. Kityk, A. Majchrowski, Opt. Mater. 25 (2004) 33.
[15] L.Y. Li, G.B. Li, Y.X. Wang, F.H. Liao, J.H. Lin, Inorg. Chem. 44 (2005) 8243.
[16] J.S. Knyrim, P. Becker, D. Johrendt, H. Huppertz, Angew. Chem. Int. Ed. 45 (2006) 48.
[17] G.K. Abdullaev, K.S. Mamedov, G.G. Dzhafarov, Kristallografiya 26 (1981) 837.
[18] A. Goriounova, P. Held, P. Becker, L. Bohatý, Acta Crystallogr. E 59 (2003) i83.
[19] A. Goriounova, P. Held, P. Becker, L. Bohatý, Acta Crystallogr. E, Structure Reports Online 60 (2004) i134.
[20] C. Sieke, T. Nikelski, T. Schleid, Z. Anorg. Allg. Chem. 628 (2002) 819.
[21] V.I. Pakhomov, G.B. Sil'nitskaya, A.V. Medvedev, B.F. Dzhurinskii, Neorg. Mater. 8 (1972) 1259;
H. Müller-Bunz, T. Nikelski, T. Schleid, Z. Naturforsch. B 58 (2003) 375.
[22] G.K. Abdullaev, K.S. Mamedov, G.G. Dzhafarov, Kristallografiya 20 (1975) 265.
[23] A. Goriounova, P. Held, P. Becker, L. Bohatý, Acta Crystllogr. E, Structure Reports Online 60 (2004) i131.
[24] H. Emme, G. Heymann, A. Haberer, H. Huppertz, Z. Naturforsch. 62b (2007) 765.
[25] H. Müller-Bunz, T. Nikeski, Th. Schleid, Z. Naturforsch. 58b (2003) 375.
[26] H. Emme, T. Nikelski, T. Schleid, R. Pöttgen, M.H. Möller, H. Huppertz, Z. Naturforsch. 59b (2004) 202.
[27] H. Emme, C. Despotopoulou, H. Huppertz, Z. Anorg. Allg. Chem. 630 (2004) 1717.
[28] H. Emme, C. Despotopoulou, H. Huppertz, Z. Anorg. Allg. Chem. 630 (2004) 2450.
[29] G. Heymann, T. Soltner, H. Huppertz, Solid State Sci. 8 (2006) 821.
[30] A. Haberer, G. Heymann, H. Huppertz, Z. Naturforsch. 62b (2007) 759.
[31] E. Parthé, Z. Kristallogr. 217 (2002) 179.
[32] J.P. Perdew, Phys. Rev. B 40 (1989) 3399.
[33] J.P. Perdew, Y. Wang, Phys. Rev. B 45 (1992) 13244.
[34] J.P. Perdew, Electronic Structure of Solids, Akademie Verlag, Berlin, Germany, 1991.
[35] J.P. Perdew, W. Yue, Phys. Rev. B 33 (1986) 8800.
[36] C.M. Zicovich-Wilson, Departamento de Fisica, Universidad Autonoma del Estado de Morelos, 〈http://www.crystal.unito.it/LoptCG/LoptCG.html〉.
[37] V.R. Saunders, R. Dovesi, C. Roetti, R. Orlando, C.M.Z. Wilson, N.M. Harrison, K. Doll, B. Civalleri, I.J. Bush, P.D. Arco, M. Llunell, CRYSTAL2003 1.0 User's Manual, 2003, August 7.
[38] H.J. Monkhorst, J.D. Pack, Phys. Rev. B 13 (1976) 5188.
[39] A.D. Becke, J. Chem. Phys. 88 (1988) 1053.
[40] J. Yang, M. Dolg, Theor. Chem. Acc. 113 (2005) 212.
[41] Energy-Consistent Pseudopotentials of the Stuttgart/aologne Group: 〈http://www.theochem.uni-stuttgart.de/pseudopotentiale/alickpse.en.html〉.
[42] M. Dolg, H. Stoll, A. Savin, H. Preuss, Theor. Chim. Acta 75 (1989) 173.
[43] M. Dolg, H. Stoll, H. Preuss, Theor. Chim. Acta 85 (1993) 441.
[44] T.H. Dunning, J. Chem. Phys. 55 (1971) 716.
[45] R. Krishnan, J.S. Binkley, R. Seeger, J.A. Pople, J. Chem. Phys. 72 (1980) 650.
[46] F. Birch, Phys. Rev. B 71 (1947) 809.
[47] F. Birch, J. Geophys. Res. 83 (1978) 1257.
[48] T. Hughbanks, R. Hoffmann, J. Am. Chem. Soc. 105 (1983) 3528.
[49] R. Dronskowski, P.E. Blöchl, J. Phys. Chem. 97 (1993) 8617.
[50] A. Grechnev, R. Ahuja, O. Eriksson, J. Phys.: Condens. Matter 15 (2003) 7751.